HHS Public Access

Author manuscript

Nano Lett. Author manuscript; available in PMC 2021 June 17.

Published in final edited form as:

Nano Lett. 2020 February 12; 20(2): 860–867. doi:10.1021/acs.nanolett.9b03175.

Massively-Parallelized, Deterministic Mechanoporation for Intracellular Delivery

Harish G. Dixit[†], **Renate Starr**[‡], **Morgan L. Dundon**[§], **Pranee I. Pairs**[§], **Xin Yang**[‡], **Yanyan Zhang**[‖], **Daniel Nampe**[†,‖], **Christopher B. Ballas**[⊥], **Hideaki Tsutsui**[†,‖,#], **Stephen J. Forman**[‡,▽], **Christine E. Brown**[‡,▽], **Masaru P. Rao**[*,†,§,‖]

[†]Department of Bioengineering, University of California – Riverside, Riverside, California 92521, United States

[‡]Department of Cancer Immunotherapy and Tumor Immunology, City of Hope Beckman Research Institute and Medical Center, Duarte, California 91010, United States

[§]Materials Science and Engineering Program, University of California – Riverside, Riverside, California 92521, United States

[‖]Department of Mechanical Engineering, University of California – Riverside, Riverside, California 92521, United States

[⊥]Division of Hematology/Oncology, Indiana University School of Medicine, Indianapolis, Indiana 46202, United States

[#]Stem Cell Center, University of California – Riverside, Riverside, California 92521, United States

[▽]Department of Hematology and Hematopoietic Cell Transplantation, City of Hope Beckman Research Institute and Medical Center, Duarte, California 91010, United States

Abstract

Microfluidic intracellular delivery approaches based on plasma membrane poration have shown promise for addressing the limitations of conventional cellular engineering techniques in a wide range of applications in biology and medicine. However, the inherent stochasticity of the poration process in many of these approaches often results in a trade-off between delivery efficiency and cellular viability, thus potentially limiting their utility. Herein, we present a novel microfluidic device concept that mitigates this trade-off by providing opportunity for deterministic mechanoporation (DMP) of cells en masse. This is achieved by the impingement of each cell upon a single needle-like penetrator during aspiration-based capture, followed by diffusive influx of exogenous cargo through the resulting membrane pore, once the cells are released by reversal of flow. Massive parallelization enables high throughput operation, while single-site poration allows for delivery of small and large-molecule cargos in difficult-to-transfect cells with efficiencies and viabilities that exceed both conventional and emerging transfection techniques. As such, DMP

[*]**Corresponding Author:** mprao@engr.ucr.edu.

The authors declare the following competing financial interest(s): M. P. R. and C. B. B. have a financial interest in Basilard BioTech.

Supporting Information

The Supporting Information is available free of charge on the ACS Publications website at DOI: 10.1021/acs.nanolett.9b03175.

Detailed description of materials and methods, as well as representative data from the control and BEP benchmarking studies (PDF)

shows promise for advancing cellular engineering practice in general and engineered cell product manufacturing in particular.

Graphical Abstract

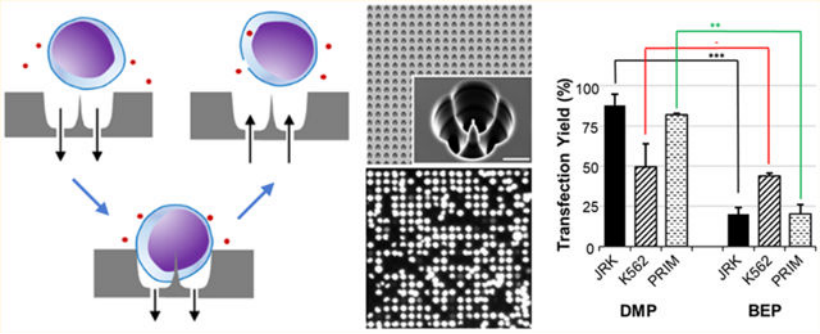

Keywords

Intracellular delivery; transfection; mechanoporation; cellular engineering; ex vivo cell therapy; cellular biomanufacturing

The safe and efficient introduction of exogenous materials into large populations of suspension cells is a key requisite for a growing number of applications based on engineered cell products. Notable examples include ex vivo cell therapies for the treatment of hematologic disorders and malignancies, wherein hematopoietic stem cells or T lymphocytes are modified outside the body to replace, correct, or add targeted genes, after which they are infused into the patient to perform their intended function (e.g., reconstitute dysfunctional cell lineages, augment stem cell transplantation, or redirect immune response to fight cancer, infection, or autoimmunity).[1–6] While viral transduction has been the most common method used for genetic manipulation in these applications, concerns such as insertional mutagenesis and scalability of vector production, among others, have driven interest in the development of nonviral transfection methods.[7–10] Similarly, these and other limitations, such as viral packaging and cargo constraints, have more broadly motivated the development of intracellular delivery techniques for a wide range of other applications in biology, medicine, and cellular biomanufacturing.[11–14]

Emerging microfluidic approaches for achieving intracellular delivery via physical disruption (i.e., poration) of the plasma membrane have shown promise for addressing many of these limitations, and within the context of suspension cells specifically recent examples include inertial microfluidic cell hydroporation (iMCH),[15] squeeze cell poration (SQZP),[16,17] acoustic shear poration (ASP),[18,19] and nanochannel electroporation (NEP).[20,21] However, although most have shown potential for scaling to the throughputs required for engineered cell product manufacturing (i.e., millions to billions of cells), many are nevertheless subject to trade-offs between delivery efficiency and cellular viability. This is particularly the case for the delivery of larger cargos (e.g., genetic constructs) to difficult-to-transfect cells that are often of interest for therapeutic applications (e.g., primary, immune, and stem cells).[22–24] One potential cause for this trade-off may lie in the inherent

stochasticity of the poration process in most of these approaches. When coupled with the need to produce pores of sufficient size to enable efficient uptake of large cargos, this may result in the formation of a multitude of large pores that ultimately compromises viability. Because both high efficiency and high viability are crucial requirements for engineered cell product manufacturing in general, and therapeutic applications in particular,[25] the need remains for the development of intracellular delivery techniques that are scalable, efficient, and able to preserve viability.

We have previously reported early results from efforts focused on addressing this need via the development of a novel microfluidic device concept that enables high throughput intracellular delivery in suspension cells through deterministic mechanoporation (DMP).[26] Herein, we expand upon this initial report by detailing results from more recent efforts focused on optimization and validation of the DMP concept. We demonstrate significant improvement in small-molecule delivery performance relative to our earlier efforts. We also report the first validation of this concept within the context of large-molecule delivery (i.e., GFP plasmid), where we observe high expression efficiency and cellular viability, thus leading to transfection yields that exceed a commercially optimized bulk electroporation protocol by over 4-fold. Finally, we demonstrate the versatility of this technique through efficient transfection of human cell lines and primary cells of relevance to ex vivo cell therapies. Collectively, these results illustrate the promise embodied in DMP for addressing critical roadblocks in the development and manufacture of engineered cell products.

As illustrated in Figure 1a, the DMP concept relies upon a unique device architecture consisting of a large array of “capture sites”, each composed of a hemispherical “capture well” with a single, submicrometer-scale, needle-like “penetrator” projecting from the bottom of the well, as well as a multiplicity of “aspiration vias” situated at the bottom of the well. Together, these features enable intracellular delivery on a single-cell basis but massively parallelized scale via the capture and release of cells en masse by aspiration flow, followed by diffusive influx of exogenous cargo through the transient plasma membrane pore produced within each cell by their impingement upon the penetrator. In doing so, this provides an opportunity for achieving deterministic poration at a single site in the plasma membrane for each cell within a large population. This therefore enables minimization of cellular damage and thus offers potential for maximizing both efficiency and viability, unlike stochastic shear-based mechanoporation approaches (e.g., SQZP, ASP, and iMCH). Furthermore, unlike other penetration-based mechanoporation techniques[27–33] the coupling of deterministic poration with aspiration-based cell manipulation provides a more facile means for rapidly and efficiently manipulating large populations of suspension cells, and importantly, collecting them immediately afterward for subsequent processing (e.g., expansion, culture/fermentation, cryopreservation, transplantation, and so forth).

Figure 1b illustrates the DMP device design, which is defined within a silicon-on-insulator substrate using conventional microfabrication processes. Key features include the following: (a) sizing of the capture wells for the intended cell type; (b) use of multiple aspiration vias within each capture well to uniformly tension the plasma membrane during capture and thus facilitate penetration; (c) use of penetrators with submicrometer tip diameters to minimize the penetration force and thus the stress upon the cells; (d) direct connection of all aspiration

vias to a large common backside aspiration port to ensure uniform flow across the array; and (e) minimized unit cell size, which enables high-density arraying of the capture sites (e.g., 2500 sites/mm^2 with total array size of 10^4 sites in the current study). Taken together, these design features simplify operation and impart intrinsic scalability, thus providing promise for meeting the needs of many engineered cell product manufacturing applications. For example, scaling to greater than 10^7 capture sites would be easily possible within the current 100 mm diameter substrates, thus enabling transfection of a sufficient numbers of cells for autologous cancer immunotherapies based on the adoptive transfer of chimeric antigen receptor (CAR) modified T cells.[34] Similarly, further scaling to greater than 10^8 capture sites would be possible within larger 300 mm substrates, thus enabling throughputs approaching those required for future allogeneic CAR T therapies, as well as a wide range of cellular biomanufacturing applications (e.g., production of therapeutic proteins, antibodies, viral vectors, and so forth).

The device fabrication process, presented in Figure 1c, was designed to enable definition of all capture site features using a single frontside mask to simplify fabrication and further ensure scalability. Using a mask pattern consisting solely of four elliptical aspiration vias per capture site, a combination of isotropic and anisotropic reactive ion etching steps was employed to define the capture site array over the large “backside aspiration port”. Scanning electron micrographs of a completed device (Figure 1d) demonstrate the realization of a uniform array of capture sites, each containing a single penetrator with submicrometer tip diameter. However, Capture well geometry is observed to deviate slightly from the intended hemispherical profile due to transport limitations during the isotropic etching step. Figure 1e illustrates the DMP device packaging, which was designed for placement on the stage of a fluorescence microscope. The package provides an open reservoir above the chip for introduction and collection of cells, as well as a port beneath the chip for fluidic communication with a programmable syringe pump for bidirectional actuation of the aspiration circuit (i.e., withdrawal mode to produce negative aspiration flow through the device for cell capture and poration, and infuse mode to produce positive aspiration flow for cell release).

In our initial report on the DMP device concept,[26] low delivery efficiencies were observed for small-molecule cargos (~15%), and subsequent investigation suggested that poor cell capture efficiency was one potential cause. As such, new studies were initiated to better understand the effect of capture flow rate on capture efficiency, and inform optimization thereof. In these new studies, an immortalized human T lymphocyte cell line (Jurkat) was selected for use due to its relevance for ex vivo cell therapies (e.g., as a model for the study and development of CAR T therapies). In order to facilitate visualization during device operation, the cells were first labeled using a membrane-permeable viability stain, Calcein Blue AM (CBAM), which is enzymatically cleaved after entry into the cytosol, thus resulting in the formation of a fluorescent dye product that is retained within cells with intact plasma membranes. The cells were then introduced into the device and subjected to varying capture flow rates, followed by manual pipetting to wash uncaptured cells from the array and remove them from the reservoir. Finally, a mosaic of fluorescence images that encompassed the entirety of the device array was collected, and capture efficiency was determined using image analysis software.

These studies showed that high capture site occupancy (71%) could be achieved at flow rates of 30 μL/min (Figure 2a). However, markedly lower occupancy was observed at higher flow rates (Figure 2b), which suggested that many of the cells in the unoccupied sites had been lysed. This was corroborated by the diminished fluorescence intensity and nonspherical morphologies seen for many of the captured cells at the higher flow rates (Figure 2b), which may have been caused by partial lysis and efflux of fluorescent CBAM molecules from the cytosol. The reduced capture efficiency observed at the lowest flow rate (Figure 2c) indicated that this too was disadvantageous, presumably because it was insufficient to retain the cells during washing. This therefore established 30 μL/min as the optimal capture flow rate for use in the remainder of the studies reported herein.

Because of the viscoelastic nature of the plasma membrane, the device operation cycle also included a negative aspiration flow pulse after the capture step to facilitate puncture, thus necessitating optimization of this parameter as well. In these studies, the Jurkats were first CBAM-stained (for visualization) and then introduced into the device and subjected to capture at the optimal 30 μL/min flow rate. Propidium iodide (PI) was also included in the device reservoir, and the cells were subjected to varying puncture flow rates after capture, followed by the removal of the uncaptured cells from the device. Although PI is typically used to quantify dead cells, in the current study it served as a model, membrane-impermeable, small-molecule exogenous cargo (668 Da) that allowed for fluorescence-based confirmation of delivery (upon intercalation with the cellular DNA). After the puncture and wash steps, the aspiration flow was reversed to release the captured cells, which were then collected and coincubated with PI and CellTracker Green (CTG) for 30 min, the former of which continued to serve as a cargo molecule, and the latter of which served as a post-DMP cellular viability marker (via retention of the enzymatically cleaved fluorescent dye product). Finally, the cells were centrifuged and resuspended for flow cytometry.

Figure 3 shows representative flow cytometry data from these studies, as well as plots summarizing the effect of puncture flow rate on cellular viability (i.e., the percentage of viable cells among the population of intact cells recovered from the device), delivery efficiency (i.e., the percentage of cells with delivered PI cargo among the population of viable intact cells), and delivery yield (i.e., the percentage of viable cells with PI cargo delivered among the population of intact cells, which is equivalent to the product of the cellular viability and delivery efficiency). It is important to note that, while commonplace, quantification in this manner does not provide means for evaluating cell losses due to the device or subsequent processing (e.g., cells lost to lysis, adhesion to cultureware surfaces, incomplete pelleting/resuspension, and so forth). High delivery efficiencies were observed for all puncture flow rates, reaching as high as 93% at 40 μL/min, thus establishing this as the optimal puncture flow rate for the Jurkats. Importantly, this also represented a 6-fold improvement in small-molecule delivery performance relative to our initial reports.[26] Although more modest cellular viabilities (and thus delivery yields) were observed, we hypothesize that this may have been an artifact resulting from the persistence of the plasma membrane pore, or transient enhancement of membrane permeability more globally, both of which would allow efflux of the fluorescent CTG products from the cytosol. However, further studies are required to confirm this conjecture, particularly because plasma

membrane repair and resealing are typically expected within a few seconds to a few minutes after mechanical injury.[35–37]

With the operational parameters optimized, we proceeded to validation of the DMP device concept within the context of large-molecule delivery. In these studies, a reporter DNA construct was included in the reservoir (GFP plasmid, 4.7 kbp), and the Jurkats were subjected to the optimal capture and puncture flow rates established earlier (i.e., 30 and 40 μL/min, respectively), followed by removal of the uncaptured cells. Afterward, the captured cells were released and collected, incubated with the plasmid for 30 min, centrifuged, resuspended in fresh media, and incubated for 12 h. The cells were then centrifuged, stained with CBAM to evaluate postincubation viability, followed by centrifugation and resuspension for flow cytometry. To evaluate the versatility of the DMP concept, the Jurkat-optimized protocol was also used to transfect an immortalized human myelogenous leukemia cell line (K-562) with the GFP plasmid. Similar to the Jurkats, the K-562 cells were selected due to their relevance for ex vivo cell therapies (e.g., as artificial antigen presenting cells for mediation of CAR T cell expansion ex vivo[38,39] or control targets for evaluation of CAR T cell product potency in vitro[34,40]). Finally, to demonstrate the potential for clinical relevance, primary human T cells were also transfected using the Jurkat-optimized DMP protocol. For the purposes of benchmarking, separate sets of all tested cell types were subjected to conventional bulk electroporation (BEP) using manufacturer-optimized protocols for each cell type, and GFP plasmid concentrations consistent with both the manufacturer recommendations and the DMP validation studies (i.e., 20 μg/mL for all cell types).

Figure 4 presents representative flow cytometry data from these studies, as well plots comparing cellular viability, transfection efficiency, and transfection yield for DMP versus BEP for all cell types. Relatively low viability and efficiency were observed for the BEP-based Jurkat transfection, thus leading to a mean transfection yield of 20%, an unsurprising result given that T cells are notoriously refractory to most conventional nonviral transfection techniques.[41] Conversely, excellent viability and efficiency were observed for DMP-based Jurkat transfection, thus resulting in a mean transfection yield of 88%, an over 4-fold improvement relative to the BEP benchmark. Importantly, this also exceeds the performance reported for other microfluidic intracellular delivery platforms for delivery of comparable GFP reporter plasmids to Jurkats specifically,[19,20] as well as other cell types more generally.[15,21,42–44] Efficient transfection of K-562 and primary human T cells using the Jurkat-optimized DMP protocol was also observed (49% and 82% yields, respectively), thus demonstrating the versatility and potential clinical relevance of the DMP device concept. However, the lower transfection yields relative to that of the Jurkats suggests opportunity for further improvement. We envision potential for doing so through refinement of the device operational parameters to accommodate any differences in the structure or injury response that may lie between the Jurkats and the other cell types.

Although further studies are required to elucidate the mechanisms underlying the high transfection yields observed herein for DMP, recent reports from other microfluidic intracellular delivery device development efforts may provide preliminary insights in this regard. For example, as discussed previously, high viability may result from the limitation of

poration to a single site in the plasma membrane, which minimizes cellular damage.[20,45] Additionally, high transfection efficiency may result from the opportunity provided for direct cytosolic delivery, which reduces potential for trapping of the exogenous cargo within endosomal or lysosomal vesicles.[16] Finally, because the penetrator length is comparable to the cell radius, this suggests potential for mechanical disruption of the nuclear envelope as well. Such disruption would be expected to facilitate intranuclear delivery and thus reduce the potential for construct degradation within the cytosol.[44]

As discussed earlier, the limitations of conventional viral and nonviral techniques for cellular engineering are well-known. Consequently, this presents wide-ranging opportunity for new nonviral techniques that can safely and efficiently introduce exogenous cargo into cells, particularly difficult-to-transfect cells such as T cells, and do so in a manner that is compatible with prevailing high-volume engineered cell product manufacturing schemes. Emerging CAR T therapies represent one compelling example in this regard, because this could enable circumvention of the looming manufacturing roadblock imposed by the current reliance upon viral transduction, which may limit the potential for extending these promising therapies beyond hematologic malignancies to the far larger population of patients with solid tumors.[46] Nonviral transfection may also provide a safer and more economical means for evaluating new tumor antigen targets relative to viral transduction,[47] thus addressing another critical roadblock to the eventual extension of CAR T therapies to solid tumor indications.[46] Although further studies are required to determine whether DMP can address these specific needs, the flexibility of this approach, combined with the encouraging data reported herein, begins to suggest promise in this regard.

In conclusion, we have reported a new microfluidic device concept for transfecting suspension cells that is specifically designed to meet the needs of engineered cell product manufacturing. The novelty of the concept lies in the opportunity it provides for deterministically porating large numbers of cells, each at a single site in their plasma membrane, and doing so in a manner that allows rapid collection of the cells for subsequent processing. Using human primary cells and cell lines of direct relevance to ex vivo cell therapies, including immune cells that are typically refractory to transfection, we show that DMP enables efficient delivery of large-molecule cargos while minimizing damage to the cell, thus allowing achievement of transfection yields that exceed both conventional and emerging nonviral transfection techniques. This, therefore, suggests that DMP may provide a new means for addressing critical roadblocks in the development and manufacture of ex vivo cell therapies based on engineered T cells (e.g., CAR T cell cancer immunotherapies). Moreover, given the inherent versatility of the DMP concept, we envision an opportunity for its eventual extension to a wide variety of other applications where progress is currently being hampered by the limitations of existing cellular engineering techniques.

Supplementary Material

Refer to Web version on PubMed Central for supplementary material.

ACKNOWLEDGMENTS

The authors thank the staff at the UC Riverside, UC Irvine, and UC Santa Barbara Nanofabrication Facilities and Dr. Brian Armstrong and Mr. Loren Quintanar, Director and Research Associate, respectively, Light Microscopy/ Digital Imaging Core, City of Hope. The authors acknowledge support for this project under Grants NIH RR026253 and GM0103973 (M.P.R. and C.B.B.), Collaborative Seed (M.P.R. and H.T.) and Proof-of-Concept (M.P.R.) Grants from the Office of Research and Economic Development at UC Riverside, and Graduate Research Fellowships from the National Science Foundation (M.L.D. and P.I.P.).

REFERENCES

(1). Naldini L Ex Vivo Gene Transfer and Correction for Cell-Based Therapies. Nat. Rev. Genet 2011, 12 (5), 301–315. [PubMed: 21445084]

(2). Scott CT; DeFrancesco L Gene Therapy's out-of-Body Experience. Nat. Biotechnol 2016, 34 (6), 600–607. [PubMed: 27281416]

(3). Aldoss I; Bargou RC; Nagorsen D; Friberg GR; Baeuerle PA; Forman SJ Redirecting T Cells to Eradicate B-Cell Acute Lymphoblastic Leukemia: Bispecific T-Cell Engagers and Chimeric Antigen Receptors. Leukemia 2017, 31 (4), 777–787. [PubMed: 28028314]

(4). Sadelain M; Riviere I; Riddell S Therapeutic T Cell Engineering. Nature 2017, 545 (7655), 423–431. [PubMed: 28541315]

(5). June CH; O'Connor RS; Kawalekar OU; Ghassemi S; Milone MC Car T Cell Immunotherapy for Human Cancer. Science 2018, 359 (6382), 1361–1365. [PubMed: 29567707]

(6). Dunbar CE; High KA; Joung JK; Kohn DB; Ozawa K; Sadelain M Gene Therapy Comes of Age. Science 2018, 359 (6372), eaan4672. [PubMed: 29326244]

(7). Qasim W; Gennery AR Gene Therapy for Primary Immunodeficiencies: Current Status and Future Prospects. Drugs 2014, 74 (9), 963–969. [PubMed: 24848753]

(8). Wang X; Riviere I Manufacture of Tumor- and Virus-Specific T Lymphocytes for Adoptive Cell Therapies. Cancer Gene Ther. 2015, 22 (2), 85–94. [PubMed: 25721207]

(9). Roh K-H; Nerem RM; Roy K Biomanufacturing of Therapeutic Cells: State of the Art, Current Challenges, and Future Perspectives. Annu. Rev. Chem. Biomol. Eng 2016, 7 (1), 455–478. [PubMed: 27276552]

(10). Roth TL; Puig-Saus C; Yu R; Shifrut E; Carnevale J; Li PJ; Hiatt J; Saco J; Krystofinski P; Li H; et al. Reprogramming Human T Cell Function and Specificity with Non-Viral Genome Targeting. Nature 2018, 559 (7714), 405–409. [PubMed: 29995861]

(11). Meacham JM; Durvasula K; Degertekin FL; Fedorov AG Physical Methods for Intracellular Delivery: Practical Aspects from Laboratory Use to Industrial-Scale Processing. J. Lab Autom 2014, 19 (1), 1–18. [PubMed: 23813915]

(12). Stewart MP; Sharei A; Ding X; Sahay G; Langer R; Jensen KF In Vitro and Ex Vivo Strategies for Intracellular Delivery. Nature 2016, 538 (7624), 183–192. [PubMed: 27734871]

(13). Marx V Cell Biology: Delivering Tough Cargo into Cells. Nat. Methods 2016, 13 (1), 37–40.

(14). Stewart MP; Langer R; Jensen KF Intracellular Delivery by Membrane Disruption: Mechanisms, Strategies, and Concepts. Chem. Rev 2018, 118 (16), 7409–7531. [PubMed: 30052023]

(15). Deng Y; Kizer M; Rada M; Sage J; Wang X; Cheon DJ; Chung AJ Intracellular Delivery of Nanomaterials Via an Inertial Microfluidic Cell Hydroporator. Nano Lett. 2018, 18 (4), 2705–2710. [PubMed: 29569926]

(16). Sharei A; Zoldan J; Adamo A; Sim WY; Cho N; Jackson E; Mao S; Schneider S; Han M-J; Lytton-Jean A; et al. A Vector-Free Microfluidic Platform for Intracellular Delivery. Proc. Natl. Acad. Sci. U. S. A 2013, 110 (6), 2082–2087. [PubMed: 23341631]

(17). Sharei A; Trifonova R; Jhunjhunwala S; Hartoularos GC; Eyerman AT; Lytton-Jean A; Angin M; Sharma S; Poceviciute R; Mao S; et al. Ex Vivo Cytosolic Delivery of Functional Macromolecules to Immune Cells. PLoS One 2015, 10 (4), No. e0118803. [PubMed: 25875117]

(18). Zarnitsyn VG; Meacham JM; Varady MJ; Hao C; Degertekin FL; Fedorov AG Electrosonic Ejector Microarray for Drug and Gene Delivery. Biomed. Microdevices 2008, 10 (2), 299–308. [PubMed: 17994280]

(19). Meacham JM; Durvasula K; Degertekin FL; Fedorov AG Enhanced Intracellular Delivery Via Coordinated Acoustically Driven Shear Mechanoporation and Electrophoretic Insertion. Sci. Rep 2018, 8 (1), 3727. [PubMed: 29487375]

(20). Boukany PE; Morss A; Liao WC; Henslee B; Jung H; Zhang X; Yu B; Wang X; Wu Y; Li L; et al. Nanochannel Electroporation Delivers Precise Amounts of Biomolecules into Living Cells. Nat. Nanotechnol 2011, 6 (11), 747–754. [PubMed: 22002097]

(21). Chang L; Gallego-Perez D; Zhao X; Bertani P; Yang Z; Chiang CL; Malkoc V; Shi J; Sen CK; Odonnell L; et al. Dielectrophoresis-Assisted 3d Nanoelectroporation for Non-Viral Cell Transfection in Adoptive Immunotherapy. Lab Chip 2015, 15 (15), 3147–3153. [PubMed: 26105628]

(22). Gresch O; Altrogge L, Transfection of Difficult-to-Transfect Primary Mammalian Cells. In Protein Expression in Mammalian Cells: Methods and Protocols; Hartley JL, Ed.; Humana Press: Totowa, NJ, 2012; pp 65–74.

(23). Zhao Y; Zheng Z; Cohen CJ; Gattinoni L; Palmer DC; Restifo NP; Rosenberg SA; Morgan RA High-Efficiency Transfection of Primary Human and Mouse T Lymphocytes Using Rna Electroporation. Mol. Ther 2006, 13 (1), 151–159. [PubMed: 16140584]

(24). Lakshmipathy U; Pelacho B; Sudo K; Linehan JL; Coucouvanis E; Kaufman DS; Verfaillie CM Efficienct Transfection of Embryonic and Adult Stem Cells. Stem Cells 2004, 22, 531–543. [PubMed: 15277699]

(25). Aijaz A; Li M; Smith D; Khong D; LeBlon C; Fenton OS; Olabisi RM; Libutti S; Tischfield J; Maus MV; et al. Biomanufacturing for Clinically Advanced Cell Therapies. Nature Biomedical Engineering 2018, 2 (6), 362–376.

(26). Zhang Y; Ballas CB; Rao MP In Towards Ultrahigh Throughput Microinjection: MEMS-Based Massively-Parallelized Mechanoporation; IEEE, 2012; pp 594–597.

(27). Shalek AK; Robinson JT; Karp ES; Lee JS; Ahn DR; Yoon MH; Sutton A; Jorgolli M; Gertner RS; Gujral TS; et al. Vertical Silicon Nanowires as a Universal Platform for Delivering Biomolecules into Living Cells. Proc. Natl. Acad. Sci. U. S. A 2010, 107 (5), 1870–1875. [PubMed: 20080678]

(28). Peer E; Artzy-Schnirman A; Gepstein L; Sivan U Hallow Nanoneedle Array and Its Utilization for Repeated Adminitration for Biomolecules to the Same Cells. ACS Nano 2012, 6 (6), 4940–4946. [PubMed: 22632128]

(29). Xie X; Xu AM; Leal-Ortiz S; Cao Y; Garner CC; Melosh NA Nanostraw-Electroporation System for Highly Efficient Intracelluar Delivery and Transfection. ACS Nano 2013, 7 (5), 4351–4358. [PubMed: 23597131]

(30). Wang Y; Yang Y; Yan L; Kwok SY; Li W; Wang Z; Zhu X; Zhu G; Zhang W; Chen X; et al. Poking Cells for Efficient Vector-Free Intracellular Delivery. Nat. Commun 2014, 5, 4466–4474. [PubMed: 25072981]

(31). Peng J; Garcia MA; Choi J.-s.; Zhao L; Chen K-J; Bernstein JR; Peyda P; Hsiao Y-S; Liu KW; Lin W-Y; et al. Molecular Recognition Enables Nanosubtrate-Mediated Delivery of Gene-Encapsulated Nanoparticles with High Efficiency. ACS Nano 2014, 8 (5), 4621–4629. [PubMed: 24708312]

(32). Chiappini C; De Rosa E; Martinez JO; Liu X; Steele J; Stevens MM; Tasciotti E Biodegradable Silicon Nanoneedles Delivering Nucleic Acids Intracellularly Induce Localized in Vivo Neovascularization. Nat. Mater 2015, 14 (5), 532–539. [PubMed: 25822693]

(33). Elnathan R; Delalat B; Brodoceanu D; Alhmoud H; Harding FJ; Buehler K; Nelson A; Isa L; Kraus T; Voelcker NH Maximizing Transfection Efficiency of Vertically Aligned Silicon Nanowire Arrays. Adv. Funct. Mater 2015, 25 (46), 7215–7225.

(34). Wang X; Naranjo A; Brown CE; Bautista C; Wong CW; Chang W-C; Aguilar B; Ostberg JR; Riddell SR; Forman SJ; et al. Phenotypic and Functional Attributes of Lentivirus-Modified Cd19-Specific Human Cd8+ Central Memory T Cells Manufactured at Clinical Scale. J. Immunother 2012, 35 (9), 689–701. [PubMed: 23090078]

(35). McNeil PL; Steinhardt RA Loss, Restoration, and Maintenance of Plasma Membrane Integrity. J. Cell Biol 1997, 137 (1), 1–4. [PubMed: 9105031]

(36). McNeil PL Repairing a Torn Cell Surface: Make Way, Lysosomes to the Rescue. Journal of Cell Science 2002, 115 (5), 873–879. [PubMed: 11870206]

(37). Andrews NW; Almeida PE; Corrotte M Damage Control: Cellular Mechanisms of Plasma Membrane Repair. Trends Cell Biol. 2014, 24 (12), 734–742. [PubMed: 25150593]

(38). Butler MO; Hirano N Human Cell-Based Artificial Antigen-Presenting Cells for Cancer Immunotherapy. Immunological Reviews 2014, 257 (1), 191–209. [PubMed: 24329798]

(39). Rushworth D; Jena B; Olivares S; Maiti S; Briggs N; Somanchi S; Dai J; Lee D; Cooper LJN Universal Artificial Antigen Presenting Cells to Selectively Propagate T Cells Expressing Chimeric Antigen Receptor Independent of Specificity. J. Immunother 2014, 37 (4), 204–213. [PubMed: 24714354]

(40). Tumaini B; Lee DW; Lin T; Castiello L; Stroncek DF; Mackall C; Wayne A; Sabatino M Simplified Process for the Production of Anti-Cd19-Car-Engineered T Cells. Cytotherapy 2013, 15 (11), 1406–1415. [PubMed: 23992830]

(41). Chicaybam L; Sodre AL; Curzio BA; Bonamino MH An Efficient Low Cost Method for Gene Transfer to T Lymphocytes. PLoS One 2013, 8 (3), No. e60298. [PubMed: 23555950]

(42). Chang L; Bertani P; Gallego-Perez D; Yang Z; Chen F; Chiang C; Malkoc V; Kuang T; Gao K; Lee LJ; et al. 3d Nanochannel Electroporation for High-Throughput Cell Transfection with High Uniformity and Dosage Control. Nanoscale 2016, 8 (1), 243–252. [PubMed: 26309218]

(43). Chang L; Gallego-Perez D; Chiang C-L; Bertani P; Kuang T; Sheng Y; Chen F; Chen Z; Shi J; Yang H; et al. Controllable Large-Scale Transfection of Primary Mammalian Cardiomyocytes on a Nanochannel Array Platform. Small 2016, 12 (43), 5971–5980. [PubMed: 27648733]

(44). Ding X; Stewart M; Sharei A; Weaver JC; Langer RS; Jensen KF High-Throughput Nuclear Delivery and Rapid Expression of DNA Via Mechanical and Electrical Cell-Membrane Disruption. Nat. Biomed Eng 2017, 1, 0039. [PubMed: 28932622]

(45). Chang L; Howdyshell M; Liao WC; Chiang CL; Gallego-Perez D; Yang Z; Lu W; Byrd JC; Muthusamy N; Lee LJ; et al. Magnetic Tweezers-Based 3d Microchannel Electroporation for High-Throughput Gene Transfection in Living Cells. Small 2015, 11 (15), 1818–1828. [PubMed: 25469659]

(46). Maus MV; Grupp SA; Porter DL; June CH Antibody-Modified T Cells: Cars Take the Front Seat for Hematologic Malignancies. Blood 2014, 123 (17), 2625–2635. [PubMed: 24578504]

(47). Zhao Y; Moon E; Carpenito C; Paulos CM; Liu X; Brennan AL; Chew A; Carroll RG; Scholler J; Levine BL; et al. Multiple Injections of Electroporated Autologous T Cells Expressing a Chimeric Antigen Receptor Mediate Regression of Human Disseminated Tumor. Cancer Res. 2010, 70 (22), 9053–9061. [PubMed: 20926399]

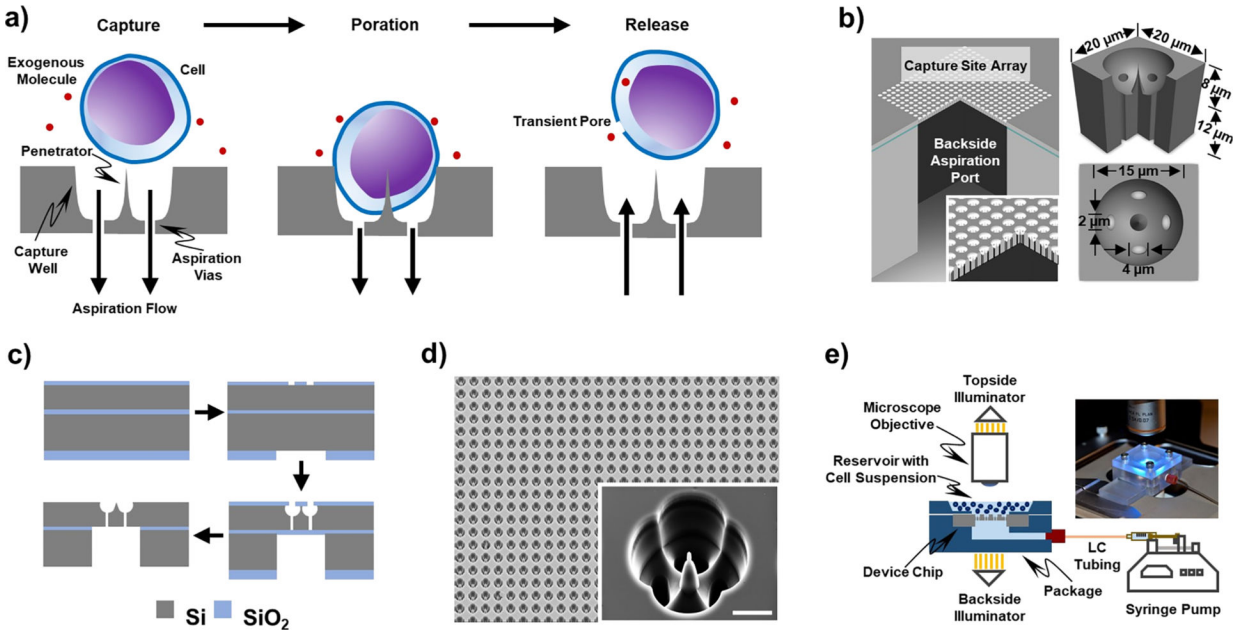

Figure 1.

DMP. (a) Concept, illustrated for a single capture site. Cells are captured using negative aspiration flow, porated by impingement upon the penetrator, and released by reversal of flow after which intracellular delivery occurs via diffusive influx of exogenous cargo through the single transient plasma membrane pore. (b) Design schematics with quarter section removed in isometric views to allow visualization of key device features. Actual devices contain a 100 × 100 array of capture sites. (c) Fabrication process. Silicon-on-insulator substrates are coated with front and backside SiO_2 layers, which are then patterned and used as masks for dry etching. (d) Scanning electron micrograph of a portion of the device array with the inset showing a higher magnification image of a single capture site (scale bar = 5 μm). (e) Schematic illustrating the packaging of the device chip, its placement upon the stage of a fluorescence microscope, and its connection to a programmable syringe pump for fluidic actuation of the aspiration circuit. The inset shows a photograph of the packaged device on the microscope stage.

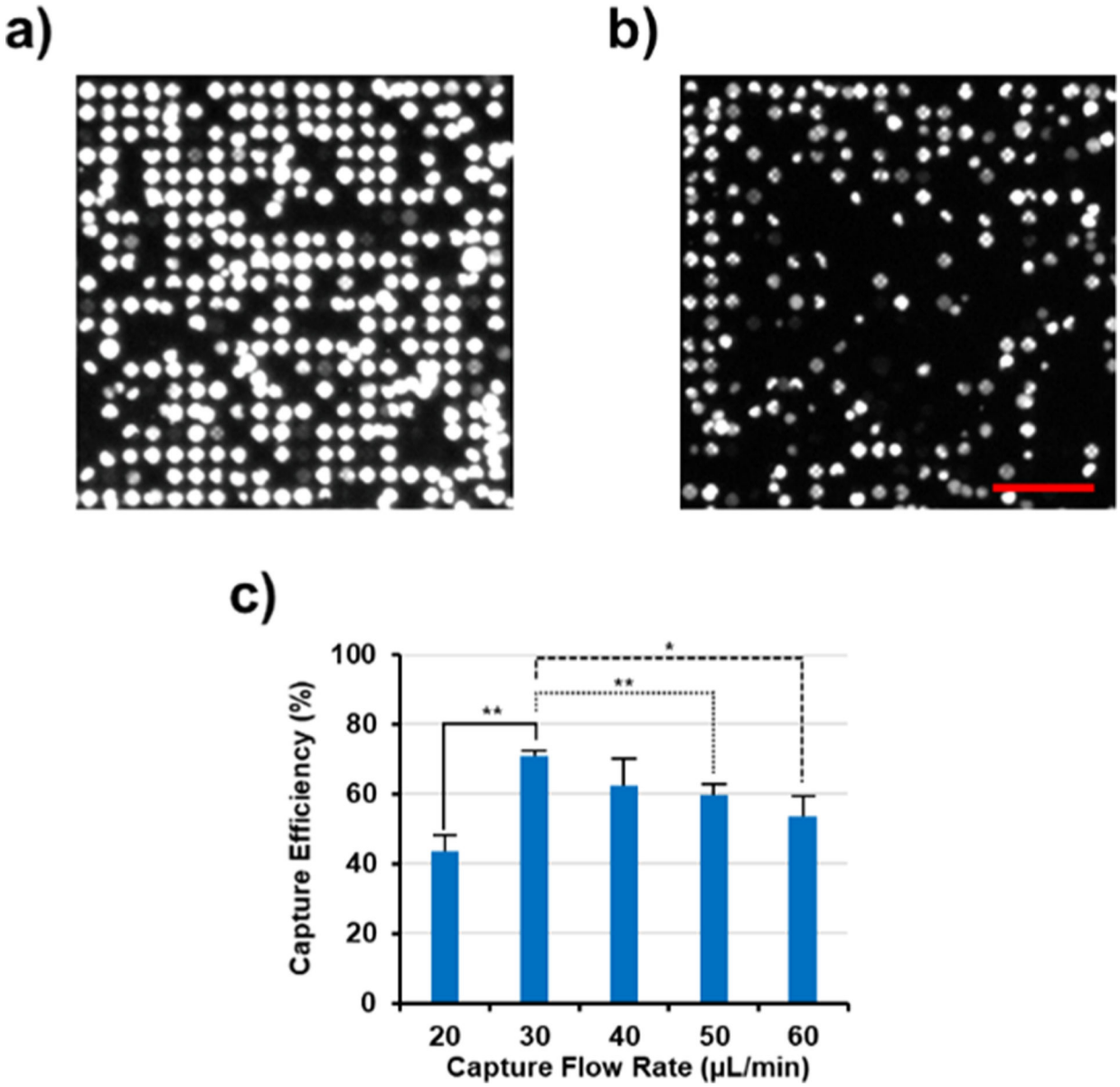

Figure 2.

Capture optimization study with Jurkats serving as a model suspension cell line. (a,b) Representative fluorescence micrographs of portions of the DMP device array showing high capture site occupancy after capture at 30 μL/min, and lower occupancy at 60 μL/min, respectively. The images share identical magnification (scale bar = 100 μm). (c) Plot of capture efficiency as a function of capture flow rate. Highest efficiency (71%) was observed at 30 μL/min (*: $p \leq 0.05$; **: $p \leq 0.01$; ***: $p \leq 0.001$; ⁻: no statistical significance). Data = mean ± standard deviation ($n = 3$).

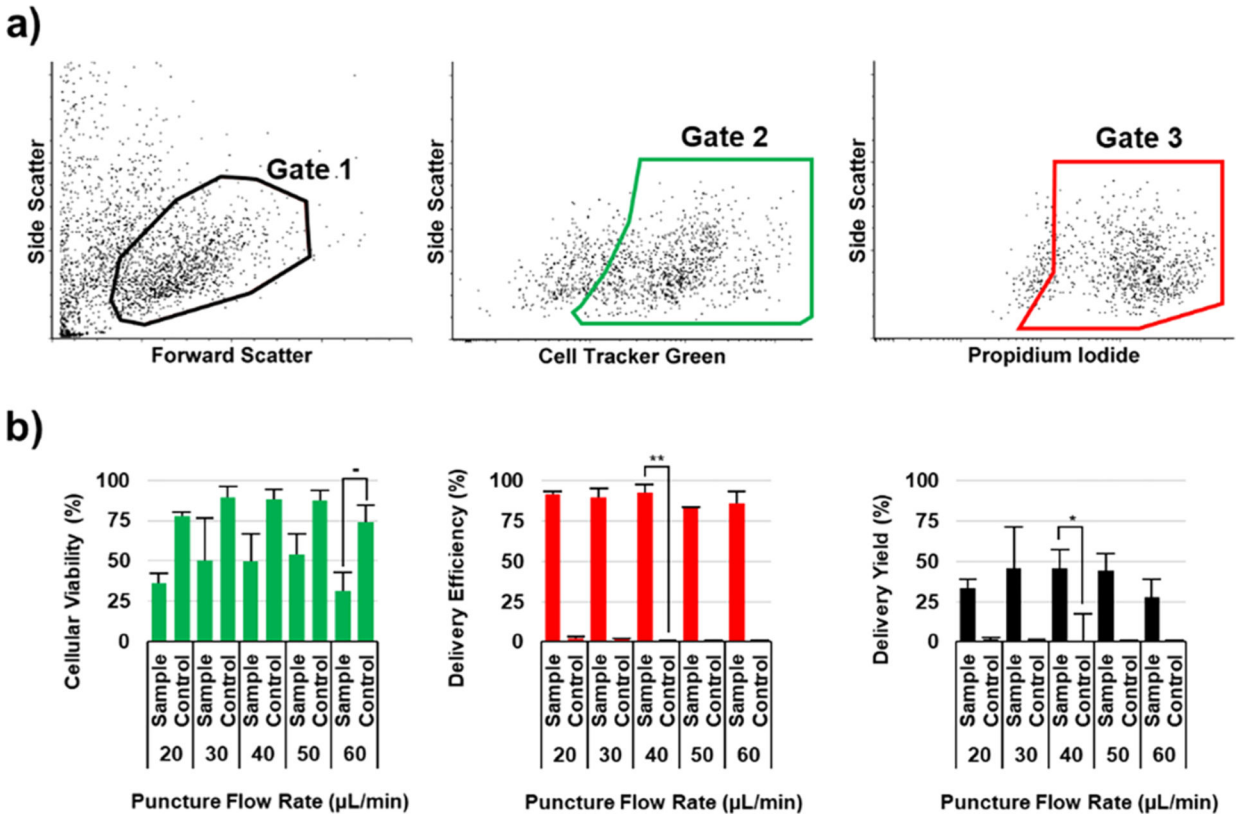

Figure 3.

Puncture optimization study using Jurkats, with propidium iodide (PI) serving as a model, membrane-impermeable, small-molecule exogenous cargo, and Cell Tracker Green (CTG) serving as a post-DMP cellular viability marker. (a) Representative flow cytometry data for cells subjected to 40 μL/min puncture flow rate. Gates 1, 2, and 3 encompass the population of intact cells (i.e., events with size and granularity consistent with intact cells), viable intact cells (i.e., CTG+), and viable intact cells with exogenous cargo delivered (i.e., both CTG+ and PI+), respectively. (b) Plots of cellular viability, delivery efficiency, and delivery yield as a function of puncture flow rate (*: $p \leq 0.05$; **: $p \leq 0.01$; ***: $p \leq 0.001$; ⁻: no statistical significance). High delivery efficiencies were seen for all conditions with the highest efficiency at 40 μL/min (93%). Gating was established using the control data presented in Figure S1 in the Supporting Information, which also showed that there was minimal passive uptake of the PI cargo and negligible autofluorescence in the spectral ranges of interest. Data = mean ± standard deviation ($n = 3$).

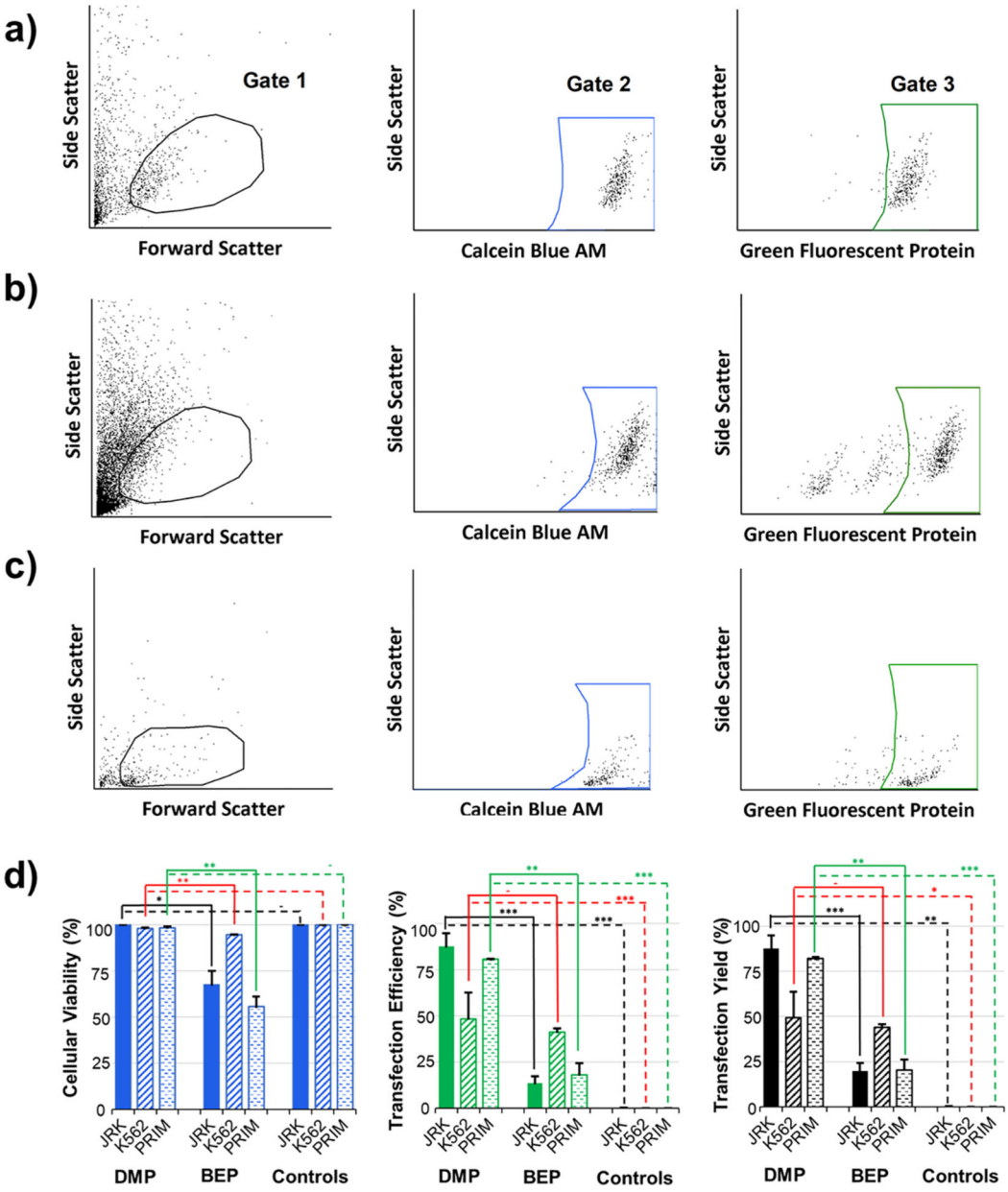

Figure 4.

DMP validation study using Jurkat, K-562, and primary human T cells with GFP plasmid serving as a model genetic construct cargo, and Calcein Blue AM (CBAM) serving as a postincubation cellular viability marker. (a–c) Representative flow cytometry data for DMP-based transfection of Jurkat, K-562, and primary human T cells, respectively. Gates 1, 2, and 3 encompass the population of intact cells, viable intact cells (i.e., CBAM+), and viable intact cells with delivery and expression of the plasmid cargo (i.e., both CBAM+ and GFP+), respectively. (d) Plots of cellular viability, transfection efficiency, and transfection yield for DMP vs conventional bulk electroporation (BEP) for Jurkat (JRKT), K-562 (K562), and primary human T cells (PRIM) (*: $p \leq 0.05$; **: $p \leq 0.01$; ***: $p \leq 0.001$; ¯: no statistical significance). High viability, efficiency, and yield were observed for DMP-transfected

Jurkats (all >87%) with mean yield over four times that of BEP (88% vs 20%, respectively). Efficient DMP-based transfection of K-562 and primary human T cells was also observed, albeit with lower yield than the Jurkats (49% and 82%, respectively, vs 88% for Jurkats). Gating was established using the control data presented in Figure S2, which also showed that there was minimal passive uptake and expression of the plasmid cargo and negligible autofluorescence in the spectral ranges of interest. Representative flow cytometry data and controls for the BEP benchmarking studies are presented in Figures S3–S5. Data = mean ± standard deviation (n = 3).